RSC Advances

PAPER

View Article Online
View Journal | View Issue

Cite this: *RSC Adv.*, 2021, **11**, 24057

Alteration of intramolecular electronic transition *via* deboronation of carbazole-based *o*-carboranyl compound and intriguing 'turn-on' emissive variation†

Seok Ho Lee, Min Sik Mun, Mingi Kim, Ji Hye Lee, Hyonseok Hwang, Wonchul Lee* and Kang Mun Lee*

The conversion of *closo*-*o*-carborane–containing compounds to the *nido*-*o*-species *via* deboronation causes photophysical changes that could be used for sensing applications. 9-Methyl-9*H*-carbazole–based *closo*- (*closo*-**Cz**) and *nido*-*o*-carboranyl (*nido*-**Cz**) compounds were prepared and fully characterised by multinuclear NMR spectroscopy and elemental analysis, and the solid-state molecular structure of *closo*-**Cz** was analysed by X-ray crystallography. Although the *closo*-compound exhibited an emissive pattern centred at λ_{em} = *ca*. 530 nm in the rigid state only (in THF at 77 K and as a film), *nido*-**Cz** demonstrated intense emission in the near-UV region (λ_{em} = *ca*. 380 nm) in both solution and film states at 298 K. The positive solvatochromic effect of *nido*-**Cz** and the results of theoretical calculations for both the *o*-carboranyl compounds supported that these emissive features originate from intramolecular charge transfer (ICT) corresponding to the *o*-carborane. Furthermore, the calculations verified that the electronic role of the *o*-carboranyl unit changed from acceptor to donor upon deboronation from *closo*-**Cz** to *nido*-**Cz**. Investigations of the radiative decay mechanisms of *closo*-**Cz** and *nido*-**Cz** according to their quantum efficiencies (Φ_{em}) and decay lifetimes (τ_{obs}) suggested that the ICT-based radiative decays of *closo*-**Cz** and *nido*-**Cz** readily occur in the film (solid) and solution state, respectively. These observations implied that the emission of *closo*-**Cz** in the solution state could be drastically enhanced by deboronation to *nido*-**Cz** upon exposure to an increasing concentration of fluoride anions. Indeed, turn-on emissive features in an aqueous solution were observed upon deboronation, strongly suggesting the potential of *closo*-**Cz** as a turn-on and visually detectable chemodosimeter for fluoride ion sensing.

Received 12th May 2021
Accepted 5th July 2021

DOI: 10.1039/d1ra03716a

rsc.li/rsc-advances

Introduction

Among the icosahedral boron-cluster compounds, *closo*-*ortho*-carborane (1,2-dicarba-*closo*-dodecaborane) has recently attracted extensive attention as a functional moiety for applied materials in the fields of optoelectronic devices[1–4] and chemodosimeter/sensors[5–17] because *o*-carborane–appended π-aromatic fluorophores can exhibit unique photophysical properties[2–4,17–65] and have reasonable thermal and electrochemical stabilities.[1–3,26,66] Such intriguing features arise from the strong electron withdrawing nature attributable to the carbon atoms of the cluster, which originates from the high polarisability of their σ-aromaticity.[6,7,67–70] These characteristics allow for the formation of electron donor (D, appended moiety)–acceptor (A, *o*-carborane) dyad systems when directly linked with π-conjugated aromatic fluorophores, which results in distinct intramolecular charge transfer (ICT) between the π-aromatic group and *o*-carborane cage during excitation and relaxation processes.[18–45,71,72] Ultimately, *closo*-*o*-carborane–possessing dyad compounds can exhibit specific luminescent characteristics based on the ICT transition.[17,34–47]

Interestingly, the ICT transition corresponding to *closo*-*o*-carborane can be definitively altered by deboronation in the presence of a nucleophilic anion such as fluoride (F^-) and hydroxide (OH^-) because the *closo*-type *o*-carborane is readily converted into the *nido*-type formation (nest-like structure, where one boron atom is removed from the icosahedron). This conversion to *nido*-*o*-carborane induces a severe counter-current ICT transition since its electronic role in the dyad system changes to a donor (D) due to the anionic nature of the *nido*-species.[5–16,73–76] Indeed, the

Department of Chemistry, Institute for Molecular Science and Fusion Technology, Kangwon National University, Chuncheon, Gangwon 24341, Republic of Korea. E-mail: kangmunlee@kangwon.ac.kr

† Electronic supplementary information (ESI) available: ^{1}H, ^{1}H{^{11}B}, ^{13}C, and ^{11}B{^{1}H} NMR spectra, X-ray crystallographic data in CIF format (CCDC – 2082043 for *closo*-**Cz**), UV-vis absorption and PL spectra for 9-methyl-9*H*-carbazole, emission decay curves, ^{1}H NMR spectral changes of *closo*-**Cz**with fluoride, and computational calculation details. CCDC 2082043. For ESI and crystallographic data in CIF or other electronic format see DOI: 10.1039/d1ra03716a

photophysical characteristics of *closo-o*-carborane appended onto various organic luminophores have been found to change dramatically during conversion to the *nido*-species in the presence of nucleophilic anions, suggesting its potential as a functional unit applicable to visualised sensory materials.[5–16]

Thus, to further investigate such changes in photophysical properties *via* the conversion of *closo-o*-carborane to the anionic *nido-o*-species by deboronation with a nucleophilic anion, we strategically designed and prepared two carbazole-based *o*-carboranyl compounds, in which *closo*- or *nido-o*-carborane is appended to the C3-position of 9-methyl-9*H*-carbazole (*closo*-**Cz** and *nido*-**Cz**, respectively, Scheme 1). To maximise the ICT-based radiative decay process, the *o*-carborane cage was substituted onto the C3-position of the carbazole moiety.[77] In addition, we also examined the potential of this system as a sensory-material scaffold to detect anionic halides by comparison of their photophysical characteristics. Detailed synthetic procedures, characterisation, and investigation of the optical properties (with theoretical calculations) of both *closo*- and *nido-o*-carboranyl compounds are described below.

Results and discussion

Synthesis and characterization

The synthetic procedure for *closo*-**Cz** and *nido*-**Cz** is shown in Scheme 1. Bromo-precursor 3-bromo-9-methyl-9*H*-carbazole (**BrCz**) was prepared as reported in the literature.[78] The acetylene compound **ACz** was obtained by the palladium-catalysed Sonogashira coupling of ethynylbenzene with **BrCz**. The 9-methyl-9*H*-carbazole–based *o*-carboranyl compound *closo*-**Cz** was then prepared *via* a cage-forming reaction[79–81] between decaborane ($B_{10}H_{14}$) and **ACz** in the presence of the weak base diethyl sulfide in moderate yield (34%). Subsequent treatment of *closo*-**Cz** with excess *n*-tetrabutylammonium fluoride (NBu_4F, TBAF) in tetrahydrofuran (THF) at 60 °C led to the conversion of the *closo*-to *nido*-carborane, *nido*-**Cz** (*nido*-form of *closo*-**Cz**)·(NBu_4) (Scheme 1).

The precursor and both *o*-carboranyl compounds were then characterised by multinuclear NMR spectroscopy (Fig. S1–S5 in the ESI†) and elemental analysis. The $^1H\{^{11}B\}$ and ^{13}C NMR spectra of *closo*-**Cz** displayed resonances corresponding to the 9-methyl-9*H*-carbazole moiety. In particular, the broad singlet peaks

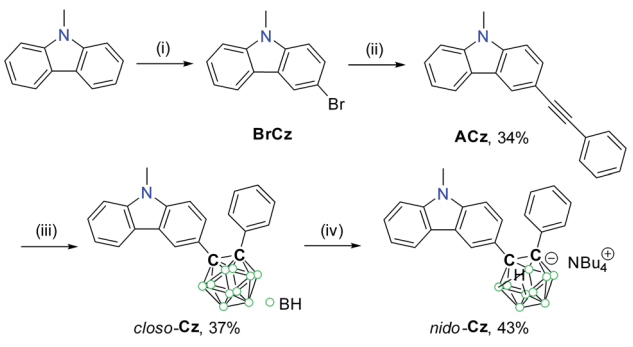

Scheme 1 Synthetic routes for the 9-methyl-9*H*-carbazole–based *closo*- and *nido-o*-carboranyl compounds (*closo*-**Cz** and *nido*-**Cz**, respectively). Reaction conditions: (i) *N*-bromosuccinmide, MeCN, 25 °C, 12 h, (ii) ethynylbenzene, CuI, $Pd(PPh_3)_2Cl_2$, toluene/NEt_3, 120 °C, 24 h. (iii) $B_{10}H_{14}$, Et_2S, toluene, 120 °C, 72 h. (iv) TBAF, THF, 60 °C, 6 h.

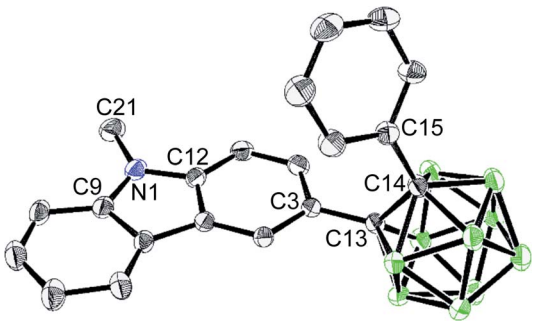

Fig. 1 X-ray crystal structure of *closo*-**Cz** (50% thermal ellipsoids, with H atoms omitted for clarity).

in the region of 3.5–2.3 ppm in the $^1H\{^{11}B\}$ NMR spectrum (assigned to 10H atoms in total) confirmed the presence of the –B*H* groups of the *o*-carborane cage. In addition, two distinct signals observed at 88 and 86 ppm in the ^{13}C NMR spectrum were attributed to the carbon atoms in *o*-carborane. The $^1H\{^{11}B\}$ NMR spectrum of *nido*-**Cz** exhibited upfield-shifted peaks relative to those of *closo*-**Cz** due to the anionic nature of *nido-o*-carborane. In particular, the broad singlet ($\delta = -1.6$ ppm) in the $^1H\{^{11}B\}$ NMR spectrum of *nido*-**Cz** clearly corresponds to the B–*H*–B bridge protons of the *nido*-carborane cages. The ^{11}B NMR signals of *closo*-**Cz** and *nido*-**Cz** detected in the regions of −3 to −11 ppm and −8 to −39 ppm further confirmed the presence of *closo*- and *nido-o*-carboranyl boron atoms, respectively.

The solid-state molecular structure of *closo*-**Cz** was examined by single-crystal X-ray diffraction (Fig. 1); the corresponding structural parameters, bond lengths, and angles are listed in Tables S1 and S2 in the ESI.† The structure of *closo*-**Cz** exhibits a perfectly planar carbazole moiety as evidenced by the sum of the angles around the N1 atom (Σ (angles around N atom centre) = 360°, Fig. 1 and Table S2†), supporting that the N centre in the structure adopts sp^2 hybridisation.

Analysis of photophysical properties in solution based on theoretical calculations

UV-vis absorption and photoluminescence (PL) measurements were performed to investigate the photophysical properties of the *closo*- and *nido-o*-carboranyl compounds (Fig. 2 and Table 1).

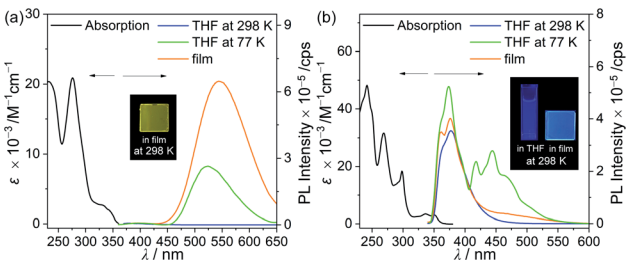

Fig. 2 UV-vis absorption (left side) and PL spectra (right side) of (a) *closo*-**Cz** (λ_{ex} = 331 nm) and (b) *nido*-**Cz** (λ_{ex} = 349 nm). Black lines: absorption spectra in THF (3.0×10^{-5} M), blue lines: PL spectra in THF (3.0×10^{-5} M) at 298 K, green lines: PL spectra in THF (3.0×10^{-5} M) at 77 K, and orange lines: PL spectra in films (5 wt% doped in PMMA) at 298 K. The insets show the emission colour in each state under irradiation by a hand-held UV lamp (λ_{ex} = 365 nm).

Table 1 Photophysical data for the 9-methyl-9*H*-carbazole–based *o*-carboranyl compounds *closo*-**Cz** and *nido*-**Cz**

			λ_{em}/nm			Φ_{em}[ad]		τ_{obs}[a]/ns		k_r[e]/10^8 s^{-1}		k_{nr}[f]/10^8 s^{-1}	
	λ_{abs}[a]/nm (ε/10^{-3} M^{-1} cm^{-1})	λ_{ex}/nm	THF[b]	77 K[a]	Film[c]	THF[b]	Film[c]	THF[b]	Film[c]	THF[b]	Film[c]	THF[b]	Film[c]
closo-**Cz**	331 (2.7), 276 (20.9)	331	—[g]	523	545	—[g]	0.41	—[g]	6.6	—	0.62	—	0.89
nido-**Cz**	349 (2.9), 298 (18.3), 269 (31.5)	349	377	376, 418, 443	376	0.24	0.13	1.4	0.69	1.7	1.9	5.4	13

[a] 3.0×10^{-5} M in THF. [b] 3.0×10^{-5} M, observed at 298 K. [c] Measured in the film state (5 wt% doped in PMMA). [d] Absolute PL quantum yield. [e] $k_r = \Phi_{em}/\tau_{obs}$. [f] $k_{nr} = k_r(1/\Phi_{em} - 1)$. [g] Not observed due to weak emission.

Both the compounds in THF demonstrated apparent low-energy absorption bands in the region of λ_{abs} = 330–350 nm, which could be assigned to a spin-allowed π–π* transition on the carbazole moiety. The low-energy absorption in a similar region (λ_{abs} = 330 and 345 nm) of the 9-methyl-9*H*-carbazole unit also distinctly supports this assignment (Fig. S6†). In addition, the absorption traces tailed to above 360 nm, indicating ICT transitions between the *o*-carborane units and carbazole moiety (see the time-dependent density functional theory (TD-DFT) results, *vide infra*). The intense absorption peaks at approximately 290 nm of both compounds could be attributed to a local π–π* transition on the carbazole group. Indeed, the spectrum of 9-methyl-9*H*-carbazole itself exhibited an absorption centred at λ_{abs} = 293 nm (Fig. S6†).

The TD-DFT calculation results for *closo*-**Cz** and *nido*-**Cz** based on the B3LYP/6-31G(d) level of theory[82] (Fig. 2) gave insights regarding the origin of the electronic transitions. Each of the ground (S_0) and first excited (S_1) states of the compounds were optimised *via* the solid-state molecular structure of *closo*-**Cz**. The integral equation formalism of the polarisable continuum model (IEFPCM) was also used to include the effect of THF as the solvent.[83] The computational results for both the *o*-carboranyl compounds in the S_0-optimised structures indicated that the lowest-energy electronic transitions are mainly associated with transitions from the highest occupied molecular orbital (HOMO) to the lowest unoccupied molecular orbital (LUMO). Intriguingly, the HOMO of *closo*-**Cz** and LUMO of *nido*-**Cz** are mainly localised on the carbazole moieties (97% for *closo*-**Cz** and 95% for *nido*-**Cz**, Tables S4 and S6†), whereas the LUMO of *closo*-**Cz** and HOMO of *nido*-**Cz** are substantially distributed over the *o*-carborane cages (30% for *closo*-**Cz** and 39% for *nido*-**Cz**). These calculation results indicate that the lowest-energy electronic absorptions of the two compounds mainly originate from sizable ICT transitions between the carbazole parts and *o*-carboranyl cages in completely different directions from each other (*closo*-**Cz**: carbazole to *o*-carborane, *nido*-**Cz**: *o*-carborane to carbazole), as well as the π–π* LE transitions on the carbazole groups.

Next, the emission properties of the two *o*-carboranyl compounds were determined by PL measurements under various conditions (Fig. 2 and Table 1). In THF at 298 K, *closo*-**Cz** exhibited no emission traces, whereas *nido*-**Cz** showed a strong emission centred at λ_{em} = 377 nm. This observation for *closo*-**Cz** results from structural fluctuations around the *closo*-*o*-carborane cages in the solution state, such as elongation of the C–C bond distance in the *o*-carborane cage, which prevent the radiative decay mechanism.[21–23,31–33,45–47,66–68] Indeed, the PL spectrum of *closo*-**Cz** in THF at 77 K exhibited intense emissive bands centred at 523 nm (Fig. 2a and Table 1) since the molecular geometry became rigid. In addition, the PL experiments for *nido*-**Cz** performed in solvents with different polarities (cyclohexane and DCM) provided further insight into the origin of the intrinsic emissive characteristics (Fig. S7†). The emission maximum of *nido*-**Cz** was slightly red-shifted upon increasing the solvent polarity (λ_{em} = 377 nm in cyclohexane to 385 nm in DCM), indicating a solvatochromic effect. These results distinctly suggest that the emission from *nido*-**Cz** is correlated to the ICT transition with the *nido*-*o*-carborane. The PL spectrum of *nido*-**Cz** in THF at 77 K exhibited carbazole-centred phosphorescence at λ_{em} = 443 nm (Fig. 2b and Table 1),[84,85] as well as slightly enhanced ICT emission compared with that at 298 K. 9-Methyl-9*H*-carbazole also showed a phosphorescent trace in the region from 420 to 480 nm in THF at 77 K (Fig. S6†).

The theoretical calculation results for the S_1 states of both the *o*-carboranyl compounds also confirmed the characteristics of the electronic transitions (Fig. 3). Each emission could be attributed to the LUMO → HOMO transition. Although the HOMO of *closo*-**Cz** and LUMO of *nido*-**Cz** are considerably localised on the carbazole moiety (>96%, Tables S4 and S6†), the

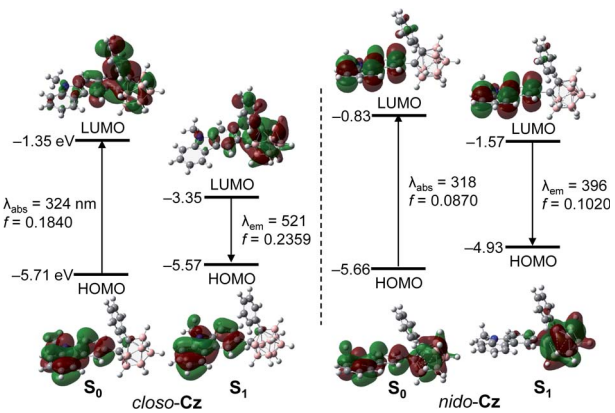

Fig. 3 Frontier molecular orbitals of *closo*-**Cz** and *nido*-**Cz** in the ground state (S_0) and first excited singlet state (S_1) with relative energies from DFT calculations (isovalue 0.04). The transition energy (in nm) was calculated using the TD-B3LYP method with the 6-31G(d) basis set.

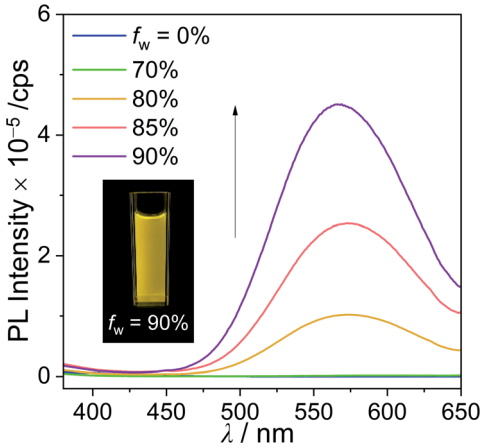

Fig. 4 PL spectra of *closo*-**Cz** (λ_{ex} = 331 nm) in THF/distilled water mixtures (3.0 × 10^{-5} M). The inset show the emission colour under irradiation by a hand-held UV lamp (λ_{ex} = 365 nm).

LUMO of *closo*-**Cz** and HOMO of *nido*-**Cz** are mostly centred on the *o*-carborane cages (>84%). These results verify that each emission is completely assignable to ICT between the carbazole and *o*-carborane units. Furthermore, these features also suggest that the intramolecular electronic role of the *o*-carborane cage could switch from acceptor (A, *closo*-**Cz**) to donor (D, *nido*-**Cz**) through deboronation of the *o*-carborane cages in the molecules.

Radiative efficiency in the solid state

The PL spectrum of *closo*-**Cz** recorded in the film state (5 wt% doped in poly(methyl methacrylate) (PMMA), solid state) also showed dramatically enhanced emissive patterns in the yellow region centred at λ_{em} = 545 nm (Fig. 2a and Table 1) compared with that in THF at 298 K. This energy region is similar to that of the PL spectrum in THF at 77 K (Fig. 2a), typically indicating ICT-based emission. Consequently, the absolute quantum efficiency (Φ_{em}) of *closo*-**Cz** in the film state was estimated to be 41% (Table 1), which is drastically higher than that in THF at 298 K (<1%). Further PL measurement of *closo*-**Cz** in a THF/water mixture (3.0 × 10^{-5} M) showed an increase in Φ_{em} in the solid state (Fig. 4). The emission at approximately 570 nm was drastically enhanced with increasing water fraction (f_w). Consequently, the maximised aggregation state in THF/water (f_w = 90%) was associated with intense yellowish emission patterns similar to those observed in the film state. These observations are characteristic of strong aggregation-induced emission from the *o*-carboranyl compound, which results in the high Φ_{em} value in the rigid state. On the other hand, *nido*-**Cz** in the film state demonstrated ICT-based emission quite similar to that in THF at 298 K. The Φ_{em} value for *nido*-**Cz** in the film state was estimated to be 13%, which is less than that in THF at 298 K (24%).

The emission decay lifetimes (τ_{obs}) of *closo*-**Cz** and *nido*-**Cz** were estimated as on the nanosecond scale (0.7–6.6 ns, Table 1 and Fig. S8 and S9†) and are thus attributable to fluorescence. The τ_{obs} and Φ_{em} values were used to calculate the radiative (k_r) and nonradiative (k_{nr}) decay rate constants (Table 1). The film-state k_r for *nido*-**Cz** (1.9 × 10^8 s^{-1}) was approximately 3 times larger than that of *closo*-**Cz** (6.2 × 10^7 s^{-1}), but k_{nr} of *closo*-**Cz** (8.9 × 10^8 s^{-1}) was considerably lower than that of *nido*-**Cz** (1.3 × 10^9 s^{-1}).

This explains the lower Φ_{em} of *nido*-**Cz** in the film state than that of *closo*-**Cz**. However, k_{nr} of *nido*-**Cz** in THF decreased to less (5.4 × 10^8 s^{-1}) than that in the film state, resulting in an enhanced Φ_{em} (24%, Table 1) in solution at 298 K.

Turn-on emissive features of *closo*-Cz *via* deboronation to *nido*-Cz

The significantly different Φ_{em} values between *closo*-**Cz** and *nido*-**Cz** in solution indicated that the *closo*-compound has the potential for use as a fluoride-detecting chemosensory material, where the emission intensity differs according to its deboronation to *nido*-**Cz**. Finally, to clarify the changes in the photoluminescence properties exhibited during the conversion of *closo-o*-carborane to the *nido*-species, we investigated the changes in the emissive patterns of *closo*-**Cz** as a function of increasing amounts of TBAF in THF (Fig. 5). The conversion process of *closo*-**Cz** to *nido*-**Cz** by reaction with fluoride anions occurs consecutively, as clearly evidenced by the changes in the specific peaks of the ^{1}H NMR spectra in THF-d^8 (Fig. S10†). The aryl protons of *closo*-**Cz** in the region from 8.2 to 7.1 ppm shifted gradually to the upfield region upon increasing the concentration of TBAF and finally became similar to the corresponding

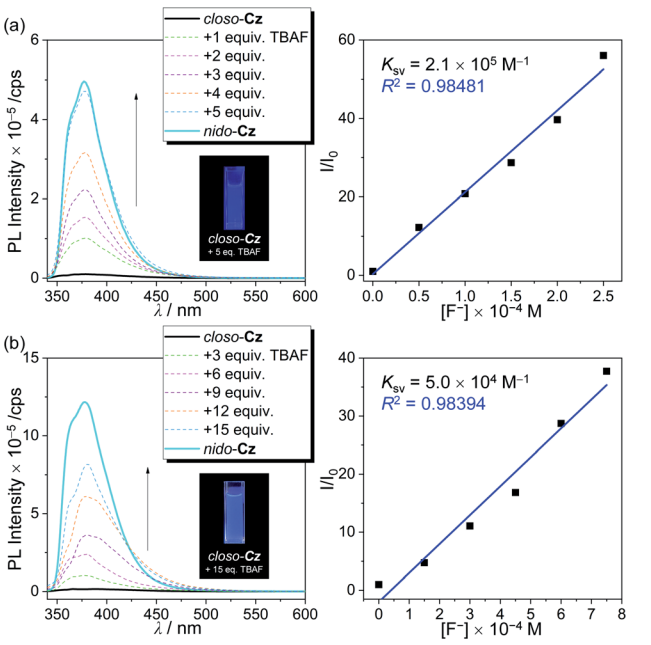

Fig. 5 Spectral changes in the fluorescence of *closo*-**Cz** (3.0 × 10^{-5} M) in (a) THF and (b) THF/H_2O mixture (1 : 1, v/v) in the presence of different amounts of TBAF after heating at 60 °C for 1 h (λ_{ex} = 349 nm) and PL spectra of *nido*-**Cz** under the same conditions. The insets are photographs of *closo*-**Cz** under a UV lamp after deboronation. The figures on the right side are linear-fitting graphs based on the Stern–Volmer equation and each Stern–Volmer constant (K_{sv}).

peaks in the spectrum of *nido*-**Cz** in THF-d^8. In particular, the broad singlet peaks at approximately −1.2 and −2.0 ppm, which were assigned to the B–*H*–B bridge protons of the *nido-o*-carborane, could be monitored upon increasing the concentration of TBAF. Furthermore, the peak assigned to molecular weight of *nido*-**Cz** species could be detected in high resolution (HR)-mass spectroscopy for *closo*-**Cz** after deboronation reaction with 5 equiv. of TBAF (Fig. S11†). In addition, infrared (IR) spectroscopy spectrum for *closo*-**Cz** was gradually changed to the spectrum for *nido*-**Cz** upon increasing the concentration of TBAF (Fig. S12†). All the spectral changes strongly suggest that the conversion of the *closo*-carborane to the *nido*-species reached nearly full conversion to *nido*-**Cz** when 5 equiv. of TBAF was used for the deboronation process. As shown in Fig. 5a, upon the addition of incremental amounts of TBAF (0 to 5 equiv.) to a THF solution of *closo*-**Cz** followed by heating at 60 °C for 1 h, the emission centred at $\lambda_{em} = 385$ nm gradually increased and eventually became similar to the emission of *nido*-**Cz**. Consequently, deboronation from *closo*-**Cz** to *nido*-**Cz** demonstrated a distinct increase in emission in the near-ultraviolet region, resulting in turn-on deep-blue emission (inset in Fig. 5a). This emissive change was accompanied by a change in the ICT-based electronic transition (*vide supra*), where the ICT transition to the carbazole (for *closo*-**Cz**) is converted to ICT to the *o*-carborane (for *nido*-**Cz**). The reaction constant (K_{sv}) of *closo*-**Cz** for deboronation was calculated as 2.1×10^5 M^{-1} by linear fitting of the fluorescence spectra with the Stern–Volmer equation (Fig. 5a, right side). Interestingly, the turn-on feature *via* deboronation of *closo*-**Cz** also occurred in an aqueous solution (THF/H_2O mixture solvent, 1 : 1, v/v, Fig. 5b). Upon addition of incremental amounts of fluoride up to 15 equiv., the intensity of the emission band at 387 nm was tremendously enhanced. The K_{sv} value of *closo*-**Cz** in an aqueous solution was estimated as a moderate 5.0×10^4 M^{-1}. All these findings indicate the potential of *closo*-**Cz** as a turn-on and visually detectable chemodosimeter for fluoride ion sensing in both organic and aqueous solutions *via* deboronation of the *closo-o*-carborane.

Experimental

General considerations

All experiments were carried out under an inert N_2 atmosphere using standard Schlenk and glovebox techniques. Anhydrous solvents (THF, toluene, and trimethylamine (NEt_3); Sigma-Aldrich) were dried by passing each solvent through an activated alumina column. Spectrophotometric-grade solvents (THF, cyclohexane, DCM, ethyl acetate (EA), *n*-hexane, toluene; Alfa Aesar) were used as received. Commercial reagents were used as received from Sigma-Aldrich (9-methyl-9*H*-carbazole, *N*-bromosuccinimide, ethynylbenzene, bis(triphenylphosphine)palladium(II) dichloride ($Pd(PPh_3)_2Cl_2$), copper(I) iodide (CuI), diethyl sulphide (Et_2S), magnesium sulphate ($MgSO_4$), TBAF, PMMA, basic aluminium oxide and Alfa Aesar (decaborane ($B_{10}H_{14}$)). 3-Bromo-9-methyl-9*H*-carbazole (BrCz) was prepared as reported in the literature.[78] The deuterated solvents (DCM-d_2 (CD_2Cl_2) and THF-d^8); Cambridge Isotope Laboratories) were dried over activated molecular sieves (5 Å). NMR spectra were recorded on a Bruker Avance 400 spectrometer (400.13 MHz for ^1H and $^1H\{^{11}B\}$, 100.62 MHz for ^{13}C, and 128.38 MHz for $^{11}B\{^1H\}$) at an ambient temperature. Chemical shifts are given in ppm and are referenced against external tetramethylsilane (Me_4Si) (^1H, $^1H\{^{11}B\}$, and ^{13}C) and $BF_3 \cdot Et_2O$ ($^{11}B\{^1H\}$). Elemental analyses, high resolution (HR)-mass spectroscopy, and infrared (IR) spectroscopy were performed on an EA3000 instrument (EuroVector), JMS-700 (JEOL), and iN10 (Thermo Scientific) at the Central Laboratory of Kangwon National University, respectively.

Synthesis of 9-methyl-3-(phenylethynyl)-9*H*-carbazole, ACz

Toluene and NEt_3 (50 mL, 2/1, v/v) were added *via* cannula to a mixture of **BrCz** (1.3 g, 5.0 mmol), CuI (95 mg, 0.50 mmol), and $Pd(PPh_3)_2Cl_2$ (0.35 g, 0.50 mmol) at 25 °C. After stirring the mixture for 30 min, ethynylbenzene (1.1 mL, 10 mmol) was added to the resulting dark brown slurry. The reaction mixture was then refluxed at 120 °C for 24 h, after which the volatiles were removed by rotary evaporation to afford a dark brown residue. The solid residue was purified by column chromatography on silica gel (eluent: DCM/*n*-hexane = 1/8, v/v, then EA/*n*-hexane = 1/10, v/v) to produce **ACz** as a yellow solid. Yield = 34% (0.38 g). ^1H NMR (CD_2Cl_2): δ 8.36 (s, 1H), 8.16 (d, $J = 7.8$ Hz, 1H), 7.72 (d, $J = 8.0$ Hz, 1H), 7.66 (d, $J = 7.8$ Hz, 2H), 7.57 (t, $J = 8.0$ Hz, 1H), 7.47 (t, $J = 8.2$ Hz, 3H), 7.42 (d, $J = 7.8$ Hz, 2H), 7.33 (t, $J = 7.4$ Hz, 1H), 3.87 (s, 3H, –C*H*$_3$). ^{13}C NMR (CD_2Cl_2): δ 141.50, 140.72, 131.49, 129.29, 128.56, 127.96, 126.31, 124.05, 123.88, 122.80, 122.29, 120.44, 119.49, 113.20, 108.89, 108.77, 91.03 (acetylene-*C*), 87.58 (acetylene-*C*), 29.10 (–*C*H$_3$). Anal. calcd for $C_{21}H_{15}N$: C, 89.65; H, 5.37; N, 4.98. Found: C, 89.51; H, 5.17; N, 4.85.

Synthesis of *closo*-Cz

To a toluene solution of $B_{10}H_{14}$ (0.26 g, 2.2 mmol) and **ACz** (0.38 g, 1.7 mmol) was added an excess amount of Et_2S (0.55 mL, 5.1 mmol) at an ambient temperature. After heating to 120 °C, the reaction mixture was stirred for a further 72 h. The solvent was removed under vacuum, and the resulting yellow solid was filtered on basic aluminium oxide in toluene. The product was recrystallised from *n*-hexane, affording *closo*-**Cz** as an ivory solid. Yield = 37% (0.25 g). $^1H\{^{11}B\}$ NMR (CD_2Cl_2): δ 8.19 (s, 1H), 8.03 (d, $J = 8.4$ Hz, 1H), 7.56 (d, $J = 8.2$ Hz, 1H), 7.51 (d, $J = 8.0$ Hz, 2H), 7.46 (d, $J = 8.0$ Hz, 1H), 7.35 (d, $J = 8.1$ Hz, 1H), 7.23 (t, $J = 8.2$ Hz, 1H), 7.13 (m, 2H), 7.08 (t, $J = 8.2$ Hz, 2H), 3.71 (s, 3H, –C*H*$_3$), 3.45 (br s, 2H, CB-B*H*), 2.62 (br s, 2H, CB-B*H*), 2.54 (br s, 4H, CB-B*H*), 2.33 (br s, 2H, CB-B*H*). ^{13}C NMR (CD_2Cl_2): δ 141.67, 141.52, 130.94, 130.80, 130.09, 128.23, 128.14, 126.57, 123.28, 122.31, 122.19, 121.14, 120.30, 119.63, 108.97, 108.00, 87.90 (CB-*C*), 86.19 (CB-*C*), 29.16 (–*C*H$_3$). $^{11}B\{^1H\}$ NMR (CD_2Cl_2): δ −3.54 (br s, 2B), −9.99 (4B), −11.80 (4B). Anal. calcd for $C_{21}H_{25}B_{10}N$: C, 63.13; H, 6.31; N, 3.51. Found: C, 62.92; H, 6.29; N, 3.44.

Synthesis of *nido*-Cz

Closo-**Cz** (26 mg, 0.075 mmol) was dissolved in a 1.0 M THF solution of *n*-tetrabutylammonium fluoride (TBAF, 0.32 mL, 0.3

mmol). THF (0.7 mL) was added *via* syringe to the mixture, and the reaction mixture was heated to reflux at 60 °C and stirred for 6 h. After cooling to room temperature, the resulting mixture was treated with distilled water (50 mL) and DCM (50 mL), and the organic portion was separated. The combined organic portions were dried over $MgSO_4$, filtered, and evaporated to dryness, affording an ivory oily residue. The residue was purified by column chromatography on silica gel (eluent: EA only). The product was recrystallised from *n*-hexane, affording *nido*-**Cz** as a white solid. Yield = 43% (20 mg). $^1H\{^{11}B\}$ NMR (CD_2Cl_2): δ 7.94 (d, J = 7.8 Hz, 1H), 7.87 (s, 1H), 7.35 (t, J = 7.5 Hz, 1H), 7.27 (t, J = 7.9 Hz, 2H), 7.19 (d, J = 7.5 Hz, 2H), 7.11 (t, J = 7.3 Hz, 1H), 6.94 (d, J = 8.4 Hz, 1H), 6.81 (t, J = 7.3 Hz, 2H), 6.71 (t, J = 7.0 Hz, 1H), 3.65 (s, 3H, –CH_3), 2.99 (m, 8H, *n*-butyl-CH_2), 2.77 (br s, 1H, CB-B*H*), 2.23 (br s, 2H, CB-B*H*), 1.99 (br s, 1H, CB-B*H*), 1.72 (br s, 2H, CB-B*H*), 1.64 (br s, 3H, CB-B*H*), 1.51 (m, 8H, *n*-butyl-CH_2), 1.37 (m, 8H, *n*-butyl-CH_2), 0.97 (t, J = 7.2 Hz, 12H, *n*-butyl-CH_3), −1.61 (br s, 1H, B–*H*–B). ^{13}C NMR (CD_2Cl_2): δ 142.33, 141.16, 139.15, 132.98, 131.98, 130.54, 126.46, 125.08, 125.04, 123.11, 122.87, 121.23, 119.98, 118.36, 108.26, 106.34, 58.92 (*n*-butyl-*C*H_2), 28.92 (–*C*H_3), 23.86 (*n*-butyl-*C*H_2), 19.71 (*n*-butyl-*C*H_2), 13.40 (*n*-butyl-*C*H_3). $^{11}B\{^1H\}$ NMR (CD_2Cl_2): δ −8.26 (2B), −14.23 (1B), −16.72 (2B), −18.97 (2B), −33.38 (1B), −35.65 (1B). Anal. calcd for $C_{37}H_{61}B_9N_2$: C, 70.41; H, 9.74; N, 4.44. Found: C, 70.21; H, 9.42; N, 4.37.

UV/vis absorption and PL measurements

Solution-phase UV/vis absorption and PL measurements for *closo*-**Cz** and *nido*-**Cz** were performed in degassed THF using a 1 cm quartz cuvette (3.0×10^{-5} M) at 298 K. PL measurements were also carried out in THF at 77 K, in THF/water mixtures, and in the film state (5 wt% doped in PMMA on a 15 mm × 15 mm quartz plate (thickness = 1 mm)). The absolute PL quantum yields (Φ_{em}) for the THF/water mixture and film samples were obtained using an absolute PL quantum yield spectrophotometer (FM-SPHERE, 3.2-inch internal integrating sphere on FluoroMax-4P, HORIBA) at 298 K. The fluorescence decay lifetimes of the films were measured at 298 K using a time-correlated single-photon counting (TCSPC) spectrometer (FLS920, Edinburgh Instruments) at the Central Laboratory of Kangwon National University. The TCSPC spectrometer was equipped with a pulsed semiconductor diode laser excitation source (EPL, 375 ps) and a microchannel plate photomultiplier tube (MCP-PMT, 200–850 nm) detector.

X-ray crystallographic analysis

A single X-ray quality crystal of *closo*-**Cz** was grown from a DCM/*n*-hexane mixture. The single crystals were coated with paratone oil and mounted on a glass capillary. Crystallographic measurements were performed using a Bruker D8QUEST diffractometer with graphite-monochromatised Mo-Kα radiation (λ = 0.71073 Å) and a CCD area detector. The structure of *closo*-**Cz** was assessed using direct methods, and all non-hydrogen atoms were subjected to anisotropic refinement with the full-matrix least-squares method on F^2 using the SHELXTL/PC software package. The X-ray crystallographic data for *closo*-**Cz** are available in CIF format (CCDC 2082043). Hydrogen atoms were placed at their geometrically calculated positions and refined using a riding model on the corresponding carbon atoms with isotropic thermal parameters. The detailed crystallographic data are given in Tables S1 and S2.†

Computational calculations

The optimised geometries for the ground (S_0) and first excited (S_1) states of both *closo*-**Cz** and *nido*-**Cz** in THF were obtained at the B3LYP/6-31G(d,p) level of theory.[82] The vertical excitation energies for the optimised S_0 geometries and the optimised geometries of the S_1 states were calculated using TD-DFT at the same level of theory.[86] Solvent effects were evaluated using the self-consistent reaction field based on IEFPCM with THF as the solvent.[83] All geometry optimisations were performed using the Gaussian 16 program.[87] The percent contributions of the groups in the molecules to each molecular orbital were calculated using the GaussSum 3.0 program.[88]

Conclusions

We successfully synthesised and fully characterised the 9-methyl-9*H*-carbazole–based *closo*- and *nido*-*o*-carboranyl compound *closo*-**Cz** and *nido*-**Cz**. *Nido*-**Cz** showed a distinct emission band in THF at 298 K centred at λ_{em} = *ca.* 380 nm, which was attributed to an ICT transition because *nido*-*o*-carborane is an electronic donor, whereas *closo*-**Cz** did not exhibit any emissive trace. This apparent difference in emissive characteristics in the solution state suggested that the emission intensity of *closo*-**Cz** in solution could be drastically enhanced by deboronation to *nido*-**Cz** upon exposure to a nucleophilic anion. Consequently, the emissive turn-on feature of *closo*-**Cz** was observed in both organic and aqueous solutions upon increasing the concentration of fluoride anions. Moreover, a moderate reactivity ($K_{sv} = 5.0 \times 10^4$ M^{-1}) towards fluoride was estimated in an aqueous solution. All these findings strongly indicate that *closo*-**Cz** has the potential for use as a turn-on and visually detectable chemodosimeter for fluoride ion sensing.

Conflicts of interest

There are no conflicts to declare.

Acknowledgements

This work was supported by the National Research Foundation of Korea (NRF) grant (NRF-2020R1A2C1006400 for K. M. Lee, and 2020R1I1A1A01073381 for J. H. Lee) funded by the Ministry of Science and ICT and Ministry of Education.

References

1 V. I. Bregadze, *Chem. Rev.*, 1992, **92**, 209–223.
2 K.-R. Wee, Y.-J. Cho, S. Jeong, S. Kwon, J.-D. Lee, I.-H. Suh and S. O. Kang, *J. Am. Chem. Soc.*, 2012, **134**, 17982–17990.
3 R. Furue, T. Nishimoto, I. S. Park, J. Lee and T. Yasuda, *Angew. Chem., Int. Ed.*, 2016, **55**, 7171–7175.

4 J. Guo, D. Liu, J. Zhang, J. Zhang, Q. Miao and Z. Xie, *Chem. Commun.*, 2015, **51**, 12004–12007.
5 M. Eo, M. H. Park, T. Kim, Y. Do and M. G. Lee, *Polymer*, 2013, **54**, 6321–6328.
6 J. O. Huh, H. Kim, K. M. Lee, Y. S. Lee, Y. Do and M. H. Lee, *Chem. Commun.*, 2010, **46**, 1138–1140.
7 K. M. Lee, J. O. Huh, T. Kim, Y. Do and M. H. Lee, *Dalton Trans.*, 2011, **40**, 11758–11764.
8 M. A. Fox, W. R. Gill, P. L. Herbertson, J. A. H. MacBride, K. Wade and H. M. Colquhoun, *Polyhedron*, 1996, **15**, 565–571.
9 J. Yoo, J.-W. Hwang and Y. Do, *Inorg. Chem.*, 2001, **40**, 568–570.
10 F. Lerouge, A. Ferrer-Ugalde, C. Viñas, F. Teixidor, R. Sillanpää, A. Abreu, E. Xochitiotzi, N. Farfán, R. Santillan and R. Núñez, *Dalton Trans.*, 2011, **40**, 7541–7550.
11 M. H. Park, K. M. Lee, T. Kim, Y. Do and M. H. Lee, *Chem.–Asian J.*, 2011, **6**, 1362–1366.
12 K. C. Song, H. Kim, K. M. Lee, Y. S. Lee, Y. Do and M. H. Lee, *Dalton Trans.*, 2013, **42**, 2351–2354.
13 D. K. You, J. H. Lee, H. Hwang, H. Kwon, M. H. Park and K. M. Lee, *Tetrahedron Lett.*, 2017, **58**, 3246–3250.
14 N. V. Nghia, J. Oh, S. Sujith, J. Jung and M. H. Lee, *Dalton Trans.*, 2018, **47**, 17441–17449.
15 N. V. Nghia, S. Jana, S. Sujith, J. Y. Ryu, S. U. Lee and M. H. Lee, *Angew. Chem., Int. Ed.*, 2018, **57**, 12483–12488.
16 H. So, M. S. Mun, M. Kim, J. H. Kim, J. H. Lee, H. Hwang, D. K. An and K. M. Lee, *Molecules*, 2020, **25**, 2413.
17 M. S. Mun, C. H. Ryu, H. So, M. Kim, J. H. Lee, H. Hwang and K. M. Lee, *J. Mater. Chem. C*, 2020, **8**, 16896–16906.
18 K. Kokado and Y. Chujo, *J. Org. Chem.*, 2011, **76**, 316–319.
19 K.-R. Wee, W.-S. Han, D. W. Cho, S. Kwon, C. Pac and S. O. Kang, *Angew. Chem., Int. Ed.*, 2012, **51**, 2677–2680.
20 L. Weber, J. Kahlert, R. Brockhinke, L. Böhling, A. Brockhinke, H.-G. Stammler, B. Neumann, R. A. Harder and M. A. Fox, *Chem.–Eur. J.*, 2012, **18**, 8347–8357.
21 L. Weber, J. Kahlert, R. Brockhinke, L. Böhling, J. Halama, A. Brockhinke, H.-G. Stammler, B. Neumann, C. Nervi, R. A. Harder and M. A. Fox, *Dalton Trans.*, 2013, **42**, 10982–10996.
22 L. Weber, J. Kahlert, L. Böhling, A. Brockhinke, H.-G. Stammler, B. Neumann, R. A. Harder, P. J. Low and M. A. Fox, *Dalton Trans.*, 2013, **42**, 2266–2281.
23 S. Kwon, K.-R. Wee, Y.-J. Cho and S. O. Kang, *Chem.–Eur. J.*, 2014, **20**, 5953–5960.
24 H. J. Bae, H. Kim, K. M. Lee, T. Kim, Y. S. Lee, Y. Do and M. H. Lee, *Dalton Trans.*, 2014, **43**, 4978–4985.
25 H. Naito, Y. Morisaki and Y. Chujo, *Angew. Chem., Int. Ed.*, 2015, **54**, 5084–5087.
26 R. Núñez, M. Tarrés, A. Ferrer-Ugalde, F. Fabrizi de Biani and F. Teixidor, *Chem. Rev.*, 2016, **116**, 14307–14378.
27 B. H. Choi, J. H. Lee, H. Hwang, K. M. Lee and M. H. Park, *Organometallics*, 2016, **35**, 1771–1777.
28 H. Naito, K. Nishino, Y. Morisaki, K. Tanaka and Y. Chujo, *J. Mater. Chem. C*, 2017, **5**, 10047–10054.
29 K. Nishino, K. Uemura, K. Tanaka, Y. Morisaki and Y. Chujo, *Eur. J. Org. Chem.*, 2018, **12**, 1507–1512.
30 H. Mori, K. Nishino, K. Wada, Y. Morisaki, K. Tanaka and Y. Chujo, *Mater. Chem. Front.*, 2018, **2**, 573–579.
31 I. Nar, A. Atsay, A. Altındal and E. Hamuryudan, *Inorg. Chem.*, 2018, **57**, 2199–2208.
32 H. Jin, H. J. Bae, S. Kim, J. H. Lee, H. Hwang, M. H. Park and K. M. Lee, *Dalton Trans.*, 2019, **48**, 1467–1476.
33 J. Ochi, K. Tanaka and Y. Chujo, *Angew. Chem., Int. Ed.*, 2020, **59**, 9841–9855.
34 K.-R. Wee, Y.-J. Cho, J. K. Song and S. O. Kang, *Angew. Chem., Int. Ed.*, 2013, **52**, 9682–9685.
35 K. Nishino, H. Yamamoto, K. Tanaka and Y. Chujo, *Org. Lett.*, 2016, **18**, 4064–4067.
36 H. Naito, K. Nishino, Y. Morisaki, K. Tanaka and Y. Chujo, *Angew. Chem., Int. Ed.*, 2017, **56**, 254–259.
37 N. Shin, S. Yu, J. H. Lee, H. Hwang and K. M. Lee, *Organometallics*, 2017, **36**, 1522–1529.
38 X. Wu, J. Guo, Y. Cao, J. Zhao, W. Jia, Y. Chen and D. Jia, *Chem. Sci.*, 2018, **9**, 5270–5277.
39 J. Li, C. Yang, X. Peng, Y. Chen, Q. Qi, X. Luo, W.-Y. Lai and W. Huang, *J. Mater. Chem. C*, 2018, **6**, 19–28.
40 X. Wu, J. Guo, J. Zhao, Y. Che, D. Jia and Y. M. Chen, *Dyes Pigm.*, 2018, **154**, 44–51.
41 A. V. Marsh, N. J. Cheetham, M. Little, M. Dyson, A. J. P. White, P. Beavis, C. N. Warriner, A. C. Swain, P. N. Stavrinou and N. Heeney, *Angew. Chem., Int. Ed.*, 2018, **57**, 10640–10645.
42 H. So, J. H. Kim, J. H. Lee, H. Hwang, D. K. An and K. M. Lee, *Chem. Commun.*, 2019, **55**, 14518–14521.
43 S. Kim, J. H. Lee, H. So, J. Ryu, J. Lee, H. Hwang, Y. Kim, M. H. Park and K. M. Lee, *Chem.–Eur. J.*, 2020, **26**, 548–557.
44 S. Kim, J. H. Lee, H. So, M. Kim, M. S. Mun, H. Hwang, M. H. Park and K. M. Lee, *Inorg. Chem. Front.*, 2020, **7**, 2949–2959.
45 M. Kim, C. H. Ryu, J. H. Hong, J. H. Lee, H. Hwang and K. M. Lee, *Inorg. Chem. Front.*, 2020, **7**, 4180–4189.
46 A. Ferrer-Ugalde, A. González-Campo, C. Viñas, J. Rodríguez-Romero, R. Santillan, N. Farfán, R. Sillanpää, A. Sousa-Pedrares, R. Núñez and F. Teixidor, *Chem.–Eur. J.*, 2014, **20**, 9940–9951.
47 K. Nishino, H. Yamamoto, K. Tanaka and Y. Chujo, *Asian J. Org. Chem.*, 2017, **6**, 1818–1822.
48 B. P. Dash, R. Satapathy, E. R. Gaillard, J. A. Maguire and N. S. Hosmane, *J. Am. Chem. Soc.*, 2010, **132**, 6578–6587.
49 B. P. Dash, R. Satapathy, E. R. Gaillard, K. M. Norton, J. A. Maguire, N. Chug and N. S. Hosmane, *Inorg. Chem.*, 2011, **50**, 5485–5493.
50 A. Ferrer-Ugalde, E. J. uárez-Pérez, F. Teixidor, C. Viñas and R. Núñez, *Chem.–Eur. J.*, 2013, **19**, 17021–17030.
51 T. Kim, H. Kim, K. M. Lee, Y. S. Lee and M. H. Lee, *Inorg. Chem.*, 2013, **52**, 160–168.
52 H. J. Bae, J. Chung, H. Kim, J. Park, K. M. Lee, T.-W. Koh, Y. S. Lee, S. Yoo, Y. Do and M. H. Lee, *Inorg. Chem.*, 2014, **53**, 128–138.
53 J. Poater, M. Solà, C. Viñas and F. Teixidor, *Angew. Chem., Int. Ed.*, 2014, **53**, 12191–12195.

54 Y. H. Lee, J. Park, S.-J. Jo, M. Kim, J. Lee, S. U. Lee and M. H. Lee, *Chem.–Eur. J.*, 2015, **21**, 2052–2061.
55 S. Mukherjee and P. Thilagar, *Chem. Commun.*, 2016, **52**, 1070–1093.
56 K. O. Kirlikovali, J. C. Axtell, A. Gonzalez, A. C. Phung, S. I. Khan and A. M. Spokoyny, *Chem. Sci.*, 2016, **7**, 5132–5138.
57 L. M. A. Saleh, R. M. Dziedzic, S. I. Khan and A. M. Spokoyny, *Chem.–Eur. J.*, 2016, **22**, 8466–8470.
58 Y. O. Wong, M. D. Smith and D. V. Peryshkov, *Chem.–Eur. J.*, 2016, **22**, 6764–6767.
59 Y. Kim, S. Park, Y. H. Lee, J. Jung, S. Yoo and M. H. Lee, *Inorg. Chem.*, 2016, **55**, 909–917.
60 J. Poater, M. Solà, C. Viñas and F. Teixidor, *Chem.–Eur. J.*, 2016, **22**, 7437–7443.
61 R. Núñez, I. Romero, F. Teixidor and C. Viñas, *Chem. Soc. Rev.*, 2016, **45**, 5147–5173.
62 D. Tu, P. Leong, S. Guo, H. Yan, C. Lu and Q. Zhao, *Angew. Chem., Int. Ed.*, 2017, **56**, 11370–11374.
63 K. O. Kirlikovali, J. Axtell, K. Anderson, P. I. Djurovich, A. L. Rheingold and A. M. Spokoyny, *Organometallics*, 2018, **37**, 3122–3131.
64 K. L. Martin, J. N. Smith, E. R. Young and K. R. Carter, *Macromolecules*, 2019, **52**, 7951–7960.
65 J. Poater, C. Viñas, I. Bennour, S. Escayola, M. Solà and F. Teixidor, *J. Am. Chem. Soc.*, 2020, **142**, 9396–9407.
66 A. M. Spokoyny, C. W. Machan, D. J. Clingerman, M. S. Rosen, M. J. Wiester, R. D. Kennedy, C. L. Stern, A. A. Sarjeant and C. A. Mirkin, *Nat. Chem.*, 2011, **3**, 590–596.
67 R. Núñez, C. Viñas, F. Teixidor, R. Sillanpää and R. Kivekäs, *J. Organomet. Chem.*, 1999, **592**, 22–28.
68 F. Teixidor, R. Núñez, C. Viñas, R. Sillanpää and R. Kivekäs, *Angew. Chem., Int. Ed.*, 2000, **39**, 4290–4292.
69 F. Teixidor, R. Núñez, C. Viñas, R. Sillanpää and R. Kivekäs, *Angew. Chem.*, 2000, **112**, 4460–4462.
70 R. Núñez, P. Farràs, F. Teixidor, C. Viñas, R. Sillanpää and R. Kivekäs, *Angew. Chem., Int. Ed.*, 2006, **45**, 1270–1272.
71 H. J. Bae, H. Kim, K. M. Lee, T. Kim, M. Eo, Y. S. Lee, Y. Do and M. H. Lee, *Dalton Trans.*, 2013, **42**, 8549–8552.
72 H. Jin, S. Kim, H. J. Bae, J. H. Lee, H. Hwang, M. H. Park and K. M. Lee, *Molecules*, 2019, **24**, 201.
73 S. Sujith, E. B. Nam, J. Lee, S. U. Lee and M. H. Lee, *Inorg. Chem. Front.*, 2020, **7**, 3456–3464.
74 F. Teixidor, J. Casabó, C. Viñas, E. Sanchez, L. Escriche and R. Kivekäs, *Inorg. Chem.*, 1991, **30**, 3053–3058.
75 F. Teixidor, C. Viñas, R. Sillanpää, R. Kivekäs and J. Casabó, *Inorg. Chem.*, 1994, **33**, 2645–2650.
76 F. Teixidor, R. Núñez, C. Viñas, R. Sillanpää and R. Kivekäs, *Inorg. Chem.*, 2001, **40**, 2587–2594.
77 S. H. Lee, M. S. Mun, J. H. Lee, S. Im, W. Lee, H. Hwang and K. M. Lee, *Organometallics*, 2021, **40**, 959–967.
78 M. B. Ponce, F. M. Cabrerizo, S. M. Bonesi and R. Erra-Balsells, *Helv. Chim. Acta*, 2006, **89**, 1123–1139.
79 M. F. Hawthorne, T. E. Berry and P. A. Wegner, *J. Am. Chem. Soc.*, 1965, **87**, 4746–4750.
80 T. E. Paxson, K. P. Callahan and M. F. Hawthorne, *Inorg. Chem.*, 1973, **12**, 708–709.
81 W. Jiang, C. B. Knobler and M. F. Hawthorne, *Inorg. Chem.*, 1996, **35**, 3056–3058.
82 E. Runge and E. K. U. Gross, *Phys. Rev. Lett.*, 1984, **52**, 997–1000.
83 S. Miertuš, E. Scrocco and J. Tomasi, *Chem. Phys.*, 1981, **55**, 117–129.
84 G. D. Boutilier and J. D. Winefordner, *Anal. Chem.*, 1979, **51**, 1391–1399.
85 S. Scypinski and L. J. C. Love, *Anal. Chem.*, 1984, **56**, 331–336.
86 E. Runge and E. K. U. Gross, *Phys. Rev. Lett.*, 1984, **52**, 997–1000.
87 M. J. Frisch, G. W. Trucks, H. B. Schlegel, G. E. Scuseria, M. A. Robb, J. R. Cheeseman, G. Scalmani, V. Barone, G. A. Petersson, H. Nakatsuji, X. Li, M. Caricato, A. V. Marenich, J. Bloino, B. G. Janesko, R. Gomperts, B. Mennucci, H. P. Hratchian, J. V. Ortiz, A. F. Izmaylov, J. L. Sonnenberg, D. Williams-Young, F. Ding, F. Lipparini, F. Egidi, J. Goings, B. Peng, A. Petrone, T. Henderson, D. Ranasinghe, V. G. Zakrzewski, J. Gao, N. Rega, G. Zheng, W. Liang, M. Hada, M. Ehara, K. Toyota, R. Fukuda, J. Hasegawa, M. Ishida, T. Nakajima, Y. Honda, O. Kitao, H. Nakai, T. Vreven, K. Throssell, J. A. Montgomery, Jr., J. E. Peralta, F. Ogliaro, M. J. Bearpark, J. J. Heyd, E. N. Brothers, K. N. Kudin, V. N. Staroverov, T. A. Keith, R. Kobayashi, J. Normand, K. Raghavachari, A. P. Rendell, J. C. Burant, S. S. Iyengar, J. Tomasi, M. Cossi, J. M. Millam, M. Klene, C. Adamo, R. Cammi, J. W. Ochterski, R. L. Martin, K. Morokuma, O. Farkas, J. B. Foresman and D. J. Fox, *Gaussian 16 Revision B.01*, Gaussian. Inc., Wallingford, CT, 2016.
88 N. M. O'Boyle, A. L. Tenderholt and K. M. Langner, *J. Comput. Chem.*, 2008, **29**, 839–845.